Int. J. Heat Mass Transfer. Vol. 25, No. 4, pp. 553–561, 1982
Printed in Great Britain

0017-9310/82/040553-09 $03.00/0

AN ANALYSIS OF THE HEAT AND SOLUTE TRANSPORT DURING SOLIDIFICATION OF AN AQUEOUS BINARY SOLUTION—I. BASAL PLANE REGION

MICHAEL G. O'CALLAGHAN, ERNEST G. CRAVALHO
Massachusetts Institute of Technology, Cambridge, Mass.

and

CHARLES E. HUGGINS
Blood Bank and Transfusion Service, Massachusetts General Hospital, Boston, MA 02114, U.S.A.

(Received 29 October 1979 and in revised form 2 October 1981)

Abstract—A mathematical analysis of the steady, dendritic solidification of an aqueous binary solution has been developed. The energy and solute transport equations were solved using a simple "two-zone" technique. In this procedure, the coupled energy and solute equations are solved first in a zone near the basal plane, and then independently solved in a zone near the dendrite tips, to obtain families of temperature, concentration and dendrite shape profiles in each region. Geometric and thermodynamic matching criteria are employed to determine the specific temperature, concentration and dendrite shape profile in each region that is mutually compatible and satisfies the overall boundary conditions. Heat and mass transport phenomena near the basal plane are analyzed in the present work, while the tip region analysis and matching procedure will be accomplished in an accompanying paper.

The results of the basal region analysis indicate that solidification at a higher rate (larger basal heat flux) produces shorter dendrites that are more blunt. A non-dimensional axial similarity variable was found which describes the temperatures and concentration fields independent of the rate of freezing.

NOMENCLATURE

a, spheroidal foci coordinate [m];
a', constant in freezing point equation [K];
b', linear coefficient in freezing point equation [K-m^3/mol];
c', quadratic coefficient in freeezing point equation [K-m^6/mol^2];
C, concentration [mol/m^3];
$\mathscr{C}$, specific heat [N-m/kg-K];
d', cubic coefficient in freezing point equation [K-m^3/mol^3];
D, diffusion coefficient of solute in solvent [m^2/s];
f, fraction of volume occupied by solid or liquid;
f_s^o, value of f_s at the basal plane;
g, normalized thermal gradient at the interface [K/m];
G_c, concentration gradient at the interface [g-mol/m^4];
H, heat flux [W/m^2];
H^*, basal heat flux component due to latent heat of fusion [W/m^2];
k, thermal conductivity [W/m-K];
L, latent heat of fusion [N-m/kg];
L^*, characteristic length [m];
m, liquidus slope [K-m^3/g-mol];
$\dot{m}$, mass-flux [g-mol/m^2-s];
$\dot{q}$, energy flux [N-m/m^2-s];
r, radial coordinate [m];
R, rate of freezing [m/s];
t, time [s];
T, temperature [K];
Z, axial coordinate [m];
Z^*, $= Z/L^*$, non-dimensional axial coordinate.

Greek symbols

α, thermal diffusivity [m^2/s];
β, constant in paraboloidal equation [m^2];
γ, linear coefficient in paraboloidal equation [m];
ε, quadratic coefficient in paraboloidal equation;
ρ, density [kg/m^3].

Subscripts and superscripts

ave, average;
eut, eutectic;
f, frontal;
I, interface condition;
ℓ, liquid region;
s, solid region;
sol, solidification;
∞, free-field condition;
o, basal condition;
eq, equivalent.

INTRODUCTION

SINGLE crystals grown from the melt of a variety of metallic and organic systems frequently exhibit a fibrous sub-structure under a wide range of freezing conditions. This sub-structure is characterized by solute-rich striations oriented in the direction of interface motion separating grains of pure solid. Experimental observation of the actual solidification process under these conditions indicates that the solid–liquid interface is not smooth, but consists of elongated grains of solid, or dendrites†, extending into the liquid as shown in Fig. 1.

Chalmers [1] first recognized the tendency for dendritic solidification whenever the conditions for morphological stability of the planar solid–liquid interface are violated. These stability conditions determine which state of aggregation, solid or liquid, is thermodynamically stable in the region just ahead of the interface. If the liquid tends to remain in the liquid state, the planar interface is stable, but if it tends toward the solid state, the planar interface will undergo a transition to the dendritic morphology.

Chalmers further postulated that a sufficient condition for interface instability is the formation of a layer of constitutionally supercooled liquid [2] just adjacent to the interface. Constitutional supercooling would promote the growth of morphological perturbations on the planar interface, leading to the formation of the more complicated but more stable dendritic structure. This theory was verified experimentally by Walton *et al.* [3] and by Tiller and Rutter [4] on the Pb–Sn alloy system.

Interface stability was recently analyzed more rigorously by Mullins and Sekerka [5, 6], and Sekerka [7]. They calculated the time variation of sinusoidal perturbations introduced into the shape of the interface. Whether the perturbations grow or decay depends on the interactions of the concentration and temperature fields, on liquid–solid surface energy, and on interface kinetics. The condition for stability for an aqueous binary solution is expressed by

$$\frac{1}{2}(g_\ell + g_s) - mG_c > 0 \qquad (1)$$

where

$$g_j = \frac{2k_j}{k_s + k_\ell}\,\mathrm{d}T\frac{\mathrm{d}T_j}{\mathrm{d}Z}, j = \mathrm{s},\ \ell. \qquad (2)$$

Equation (2) represents the "conductivity-weighted" temperature gradient, and mG_c is the gradient in the liquidus temperature at the interface. Equation (1) differs from the constitutional supercooling criterion in that the stabilizing effect of the heat flux behind the interface is included.

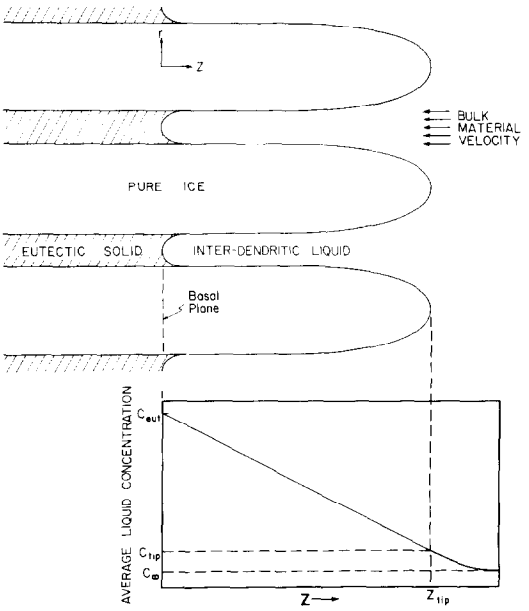

FIG. 1. Dendritic solidification geometry.

The Mullins–Sekerka stability criterion has been applied quantitatively to the freezing of aqueous binary solutions by O'Callaghan *et al.* [8]. Their results indicate that the planar interface rapidly becomes unstable during freezing except at very low freezing rates or solute concentrations. As discussed above, the unstable planar interface will transform to the dendritic morphology under these conditions.

The present work is an analysis of the heat and mass transport that accompanies the steady dendritic solidification of an aqueous binary solution. Our specific purpose is to calculate the temperature and concentration fields and the dendrite shape, length‡ and spacing. The problem will be solved using a simplified "two-zone" scheme. In this procedure, the coupled equations of solute and energy conservation are solved for two separate regions, one near the basal plane and the other near the dendrite tip, to obtain families of temperature and concentration profiles in each region. Geometric and thermodynamic matching criteria will be employed to determine the specific temperature and concentration profiles in each region that are mutually compatible and satisfy the overall boundary conditions.

TWO-ZONE FREEZING MODEL

Consider the steady dendritic solidification geometry shown in Fig. 1. In describing the dendrite shape and associated transport fields, the most convenient reference frame is that which is fixed with respect to the dendrite surface. In this reference frame, if we neglect the volume change associated with freezing, the entire field is uniformly moving at the steady solidification

†These elongations have been named "dendrites" or "cellular dendrites" by various authors. The former term will be used throughout this paper.

‡Dendrite length is defined as the distance from the foremost point to the basal plane, where the eutectic condition is attained.

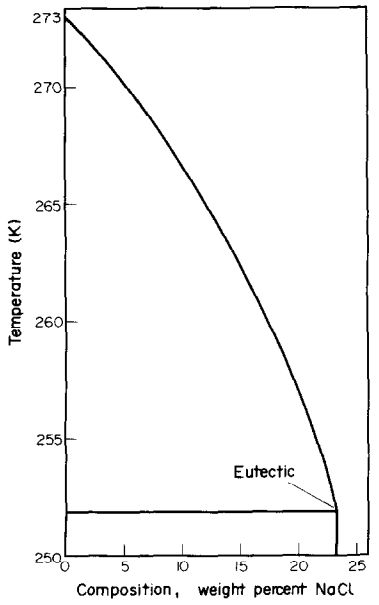

FIG. 2. $NaCl-H_2O$ phase diagram. Most electrolyte–water phase diagrams are very similar to this.

then, does so by bulk entrapment at the eutectic condition.

The approximate loci of constant temperature and concentration in the vicinity of a growing dendrite are shown in Fig. 3. These loci were constructed by applying boundary conditions of symmetry, and by considering two model solidification geometries. First, if dendrite shape and cross-sectional area were uniform, and if the dendrites were infinitely long, then the loci would be perfect planes. This situation is approximated near the basal plane, where dendrite diameter is nearly constant. In this zone, the transport fields may be well approximated as 1-dim. in the axial direction.

As the second model, if we consider isolated freely-growing dendrites, then the dendrite tip and iso-potential loci in its vicinity may be accurately described as paraboloids of revolution as indicated by Ivantsov [9] and Bolling and Tiller [10]. Paraboloids have the characteristic "nose-cone" shape illustrated in Fig. 3. Thus, the iso-potential loci near the tips of dendrites growing in close-packed array may be approximated as paraboloids of revolution. Paraboloids are 2-dim. surfaces in the circular cylinder

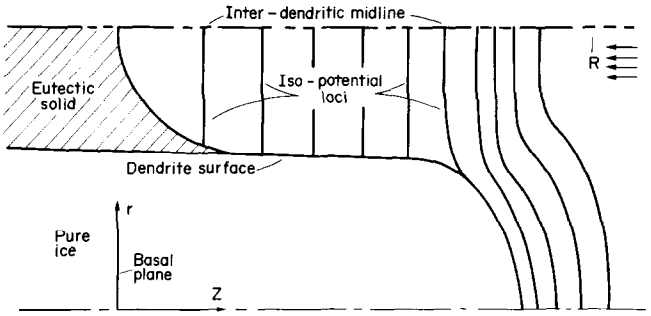

FIG. 3. Iso-potential loci (constant temperature and concentration) near a growing dendrite.

velocity R.† The crystals of pure ice extend from the basal plane (the original planar interface) into the liquid region, dividing the field into an all-liquid region, a "mushy" (two-phase) region and a pure solid region. A typical aqueous phase diagram, shown in Fig. 2, indicates that solute is completely excluded from the advancing dendrite, by virtue of the vertical solidus at 0% NaCl. This fact is confirmed by recent estimates of the equilibrium distribution coefficient of less than 10^{-4} [12]. The rejected solute enters the inter-dendritic liquid which becomes increasingly enriched as it approaches the basal plane. The upper limit on the liquid concentration is the eutectic, which has been shown to be reached at the basal plane even when the free-field concentration is a very small fraction of the eutectic [2]. Any solute that enters the solid phase,

†This volume change would give rise to relative motion between the solid and liquid regions. Its effect is assumed negligible.

coordinate system described by

$$r^2 = \beta + \gamma Z + \varepsilon Z^2 \tag{3}$$

where β, γ and ε are constants, r is the dendrite radius (assumed circular in cross-section) and Z is the axial coordinate fixed with respect to the dendrite surface. If we transform to the oblate spheroidal coordinate system defined by

$$r = a \cosh \eta \sin \theta \tag{4}$$

and

$$Z = a \sinh \eta \cos \theta, \tag{5}$$

the surfaces described by equation (3) become

$$\eta = \text{constant for } 0 \leq \theta \leq \pi. \tag{6}$$

Energy and mass transport near the dendrite tips are therefore 1-dim. when described in the oblate spheroidal coordinate system. Analysis of the tip region transport phenomena is accomplished in an accompanying paper [11].

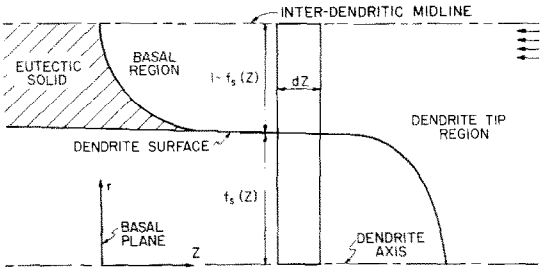

FIG. 4. Differential volume element for derivation of energy and solute transport equations.

ENERGY AND SOLUTE TRANSPORT NEAR THE DENDRITE BASE

Transport equations

As discussed above, the iso-potential loci may be assumed to be planar near the basal plane, with temperature and concentration varying only in the axial direction. Consider a differential volume element of thickness dZ located at position Z, which extends from the centerline of a dendrite to the midline of the interdendritic volume (see Fig. 4). At any position Z, the fraction of cross-sectional area occupied by solid phase is $f_s(Z)$, and the remaining fraction (occupied by liquid) is $f_\ell(Z) = 1 - f_s(Z)$.

The first law of thermodynamics applied to this control volume has three contributions: heat transfer by conduction, heat transfer by mass motion (convection), and energy generation due to solidification. The net heat transfer by conduction is found by summing the input and output terms for the liquid and solid fractions as follows:

$$\dot{q}_{\text{cond}} = k_s f_s(Z + \mathrm{d}Z)\frac{\partial T}{\partial Z}(Z + \mathrm{d}Z) + k_\ell f_\ell(Z + \mathrm{d}Z)\frac{\partial T}{\partial Z}$$

$$\times (Z + \mathrm{d}Z) - k_s f_s(Z)\frac{\partial T}{\partial Z}(Z) - k_\ell f_\ell(Z)\frac{\partial T}{\partial Z}(Z). \quad (7)$$

The convective heat flux may be determined by dividing the freezing field into the following three sections:

(a) the region extending from the dendrite centerline to $f_s(Z + \mathrm{d}Z)$;

(b) the region consisting of $\mathrm{d}f_\ell$ (which equals $\mathrm{d}f_s$);

(c) the region extending from $f_s(Z)$ to the interdendritic mid line.

In sections (a) and (c), the material does not undergo a change of phase but changes temperature only. The net convective heat flux in these two sections is given by

$$\dot{q}_{\text{conv}}(a) = R\rho_s \mathscr{C}_s f_s(Z + \mathrm{d}Z)\,[T(Z + \mathrm{d}Z) - T(Z)] \quad (8)$$

and

$$\dot{q}_{\text{conv}}(c) = R\rho_\ell \mathscr{C}_\ell f_\ell(Z)[T(Z + \mathrm{d}Z) - T(Z)]. \quad (9)$$

†Note that the latent heat of solidification will be considered separately.

The material in section (b) however, undergoes a change of phase. Since $\rho_\ell \mathscr{C}_\ell$ does not equal to $\rho_s \mathscr{C}_s$, it is necessary to consider the net convective heat flux in section (b) in two parts. First, the liquid is changed in temperature from $T(Z + \mathrm{d}Z)$ to the freezing temperature and second the solid is changed in temperature from the freezing temperature to $T(Z)$.† If we represent the freezing temperature by the average temperature in dZ given by

$$T_{\text{ave}} = \tfrac{1}{2}[T(Z + \mathrm{d}Z) + T(Z)] \quad (10)$$

then the convective energy interaction for section (b) is given by

$$\dot{q}_{\text{conv}}(b) = R\rho_\ell \mathscr{C}_\ell \mathrm{d}f_\ell[T(Z + \mathrm{d}Z) - T_{\text{ave}}] + R\rho_s \mathscr{C}_s \mathrm{d}f_\ell[T_{\text{ave}} - T(Z)]. \quad (11)$$

Adding equations (8)–(11) and rearranging, we obtain

$$\dot{q}_{\text{conv}} = R\rho_s \mathscr{C}_s\{T(Z + \mathrm{d}Z)f_s(Z + \mathrm{d}Z) - T(Z)f_s(Z)\} + R\rho_\ell \mathscr{C}_\ell\{T(Z + \mathrm{d}Z)f_\ell(Z + \mathrm{d}Z) - T(Z)f_\ell(Z)\} - R(\rho_s \mathscr{C}_s - \rho_\ell \mathscr{C}_\ell)\tfrac{1}{2}[T(Z + \mathrm{d}Z) + T(Z)]\,\mathrm{d}f_s. \quad (12)$$

Finally, the rate of energy generation within the control volume is given by the rate of liberation of the latent heat of fusion

$$\dot{q}_{\text{gen}} = R\{f_s(Z + \mathrm{d}Z) - f_s(Z)\}\rho_s L. \quad (13)$$

By assuming that the interface speed is constant, we may perform a steady state analysis. Therefore, the net rate of energy transfer into the control volume must be zero. Adding equations (7), (12) and (13), dividing by dZ and taking the limit as $\mathrm{d}Z \to 0$, we obtain

$$\{k_s f_s + k_\ell(1 - f_s)\}T'' + \{(k_s - k_\ell)f_s' + R\rho_s \mathscr{C}_s f_s + R\rho_\ell \mathscr{C}_\ell(1 - f_s)\}T' - R\rho_s L f_s' = 0 \quad (14)$$

where the superscript prime represents differentation with respect to Z.

Conservation of solute may be written for the same control volume, but since solute is completely rejected from the solid phase, diffusion and convection of solute occur only in the liquid. The net diffusive mass flux is given by

$$\dot{m}_{\text{diff}} = D f_\ell(Z + \mathrm{d}Z)\frac{\partial C}{\partial Z}(Z + \mathrm{d}Z) - D f_\ell(Z)\frac{\partial C}{\partial Z}(Z). \quad (15)$$

The net convective mass flux is given by an expression similar to equation (12)

$$\dot{m}_{\text{conv}} = R f_\ell(Z + \mathrm{d}Z)C(Z + \mathrm{d}Z) - R f_\ell(Z)C(Z). \quad (16)$$

In the steady state the net rate of accumulation of mass in the control volume must be zero. Summing equations (15) and (16), dividing by dZ and taking the limit as $\mathrm{d}Z \to 0$, we obtain

$$D(1 - f_s)C'' + \{R(1 - f_s) - Df_s'\}C' - (Rf_s')C = 0. \quad (17)$$

The rate of freezing, R of aqueous solutions and metallic alloys is a monotonic function of the thermal supercooling at the interface [1]. Typically, the normal growth rate near the basal plane in the present case is on the order of 10^{-4}m/s, and the resulting interface supercooling will be less than 10^{-1} K. Although this quantity is important from a kinetics viewpoint, it is clearly negligible in terms of energy transport. The solid and liquid at any axial position are therefore assumed at thermodynamic equilibrium, with the temperature–concentration relationship approximated by

$$T(Z) = a' + b'C(Z) + c'C^2(Z) + d'C^3(Z). \quad (18)$$

This relationship results from a power series curve fit of equilibrium freezing point data of the solute under consideration.

Equations (14) and (17) may be made axially nondimensional by using the transformation

$$z^* = Z/L^* \quad (19)$$

where

$$L^* = \frac{(k_s - k_\ell)f_s^\circ + k_\ell}{R[(\rho_s\mathscr{C}_s - \rho_\ell\mathscr{C}_\ell)f_s^\circ + \rho_\ell\mathscr{C}_\ell]}. \quad (20)$$

Transforming equation (14) to the Z^* coordinate system, we have

$$\left[\frac{(k_s - k_\ell)f_s + k_\ell}{(k_s - k_\ell)f_s^\circ + k_\ell}\right]\left[\frac{(\rho_s\mathscr{C}_s - \rho_\ell\mathscr{C}_\ell)f_s^\circ + (\rho_\ell\mathscr{C}_\ell)}{(\rho_s\mathscr{C}_s - \rho_\ell\mathscr{C}_\ell)f_s + (\rho_\ell\mathscr{C}_\ell)}\right]\frac{d^2T}{dZ^{*2}}$$

$$+\left[\frac{(k_s - k_\ell)}{(k_s - k_\ell)f_s^\circ + k_\ell}\frac{(\rho_s\mathscr{C}_s - \rho_\ell\mathscr{C}_\ell)f_s^\circ + \rho_\ell\mathscr{C}_\ell}{(\rho_s\mathscr{C}_s - \rho_\ell\mathscr{C}_\ell)f_s + \rho_\ell\mathscr{C}_\ell}\frac{df_s}{dZ^*} + 1\right]$$

$$\times\frac{dT}{dZ^*} + \left[\frac{-\rho_s L}{(\rho_s\mathscr{C}_s - \rho_\ell\mathscr{C}_\ell)f_s + \rho_\ell\mathscr{C}_\ell}\right]\frac{df_s}{dZ^*} = 0. \quad (21)$$

Similarly, transformation of the mass transfer equation yields

$$\frac{d^2C}{dZ^{*2}} + \left[\frac{(k_s - k_\ell)f_s^\circ + k_\ell}{D[(\rho_s\mathscr{C}_s - \rho_\ell\mathscr{C}_\ell)f_s^\circ + \rho_\ell\mathscr{C}_\ell]} - \frac{1}{(1 - f_s)}\frac{df_s}{dZ^*}\right]$$

$$\times\frac{dC}{dZ^*} + \left[\frac{(k_s - k_\ell)f_s^\circ + k_\ell}{D[(\rho_s\mathscr{C}_s - \rho_\ell\mathscr{C}_\ell)f_s^\circ + \rho_\ell\mathscr{C}_\ell]}\right]$$

$$\times\frac{df_s}{dZ^*}C = 0. \quad (22)$$

Note that the interface speed R does not appear in either equation (21) or (22). For specific free-field conditions (C_∞, T_∞), the transport fields and dendrite shape are identical for all interface speeds when described in the Z^* coordinate system.

Boundary conditions

Simultaneous solution of equations (18), (21), and (22) requires the specification of three independent boundary conditions. The boundary conditions that are presumed known in the present case are given by

$$T(Z^* = 0) = T_{eut}, \quad (23)$$

$$C(Z^* \to \infty) = C_\infty, \quad (24)$$

$$T(Z^* \to \infty) = T_\infty. \quad (25)$$

Equation (23) is obtained by definition of the eutectic condition at the basal plane, while equations (24) and (25) express known free-field conditions.

These boundary conditions, together with the transport equations derived above, comprise a complete mathematical statement of the basal transport problem which may be theoretically solved by analysis. However, in order to numerically solve the complete set of equations using the "two-zone" solution technique, it will be necessary to replace equations (24) and (25) with boundary conditions that apply at the basal plane. The basal concentration boundary condition may be replaced by

$$f_s^\circ = 1 - \frac{C_\infty}{C_{eut}} \quad (26)$$

which is obtained by applying conservation of solute to the entire solidification field, and noting that

$$C(Z^* = 0) = C_{eut}. \quad (27)$$

The boundary condition stated by equation (25) will be met by an iterative procedure which is detailed in the accompanying paper. Basically, the procedure consists of assuming a basal temperature gradient dT/dZ^* (which is not known *a priori*), and then calculating the resulting free-field temperature T_∞ by solving the complete set of transport equations.† If the calculated T_∞ is not acceptably close to the known free-field temperature, then an adjustment is made in the basal temperature gradient and the entire process is repeated. Obviously, this procedure can be applied only after the tip region analysis has been developed and the appropriate stability and matching criteria applied.

In order to demonstrate the character of the basal region transport fields, a parameter study will be accomplished, in which several reasonable values of basal temperature gradient (and equivalently basal heat flux) will be assumed. The basal heat flux consists of two components: the heat flux required to remove the latent heat of fusion, and the sensible heat flux needed to change the liquid to the freezing temperature and subcool the solid to the eutectic condition. It is possible to calculate a limited range of basal heat fluxes within which the actual heat flux must lie. This range is given by

†This procedure has been called a "shooting method" in classical numerical analysis.

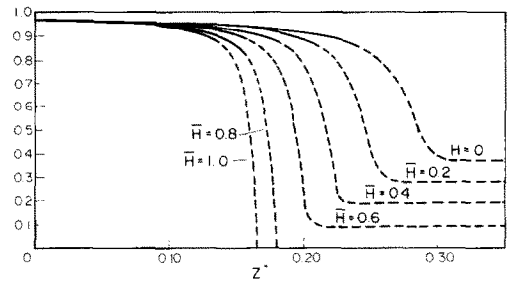

FIG. 5. Non-dimensional dendrite shape profiles as a function of $\bar{H} = [H(Z^* = 0) - H^*]/H^{max}_{sensible}$.

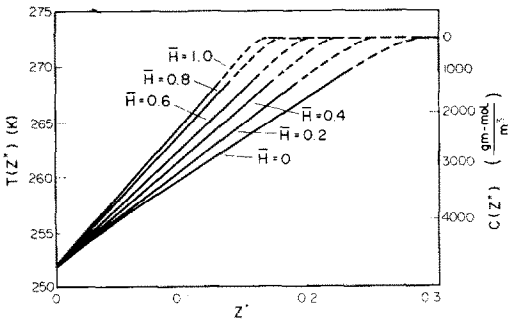

FIG. 6. Temperature and concentrations as a function of $\bar{H} = [H(Z^* = 0) - H^*]/H^{max}_{sensible}$. Both quantities may be read from the same profiles, using the left and right axes respectively.

$$H^* < H(Z^* = 0) < H^* + H^{max}_{sensible} \tag{28}$$

where

$$H^* = R\rho_s L f_s(Z^* = 0) \tag{29}$$

which represents the rate of liberation of the latent heat of fusion, and $H^{max}_{sensible}$ is the maximum value of the sensible heat flux. This maximum may be estimated by assuming that the liquid is sensibly cooled to the eutectic temperature before freezing takes place, and is given by

$$H^{max}_{sensible} = R\rho_\ell \mathscr{C}_\ell (T_\infty - T_{eut}). \tag{30}$$

†Temperature and concentration may be plotted on the same axes by virtue of equation (18).

Using material properties for saline with $T_\infty = 273.15$ K in equations (29) and (30), we find that the maximum sensible heat flux is about 20% of the solidification heat flux under typical conditions.

Finally, let us define a non-dimensional basal heat flux given by

$$\bar{H} = \frac{H(Z^* = 0) - H^*}{H^{max}_{sensible}}. \tag{31}$$

This parameter is the ratio of the sensible component of the basal heat flux to the maximum possible value of the sensible heat flux. It is clear from equations (28), (29), and (30) that $\bar{H} < 1$ and that complete removal of the latent heat of solidification occurs only when $\bar{H} > 0$.

RESULTS AND DISCUSSION

The temperature (and concentration†), temperature gradient, and dendrite shape profiles resulting from the numerical integration of the solidification equations is shown in Figs. 5–7 for the freezing of saline at various values of basal heat flux. Values of physical constants are listed in Table 1.

The dendrite shape profiles, shown in Fig. 5 are characterized by a slightly negative slope near the basal plane followed by a sharp decrease near the presumed location of the dendrite tip. The imposed assumption of planar isotherms and isoconcentrates, however, is valid only where the dendrite cross-sectional area does not show strong axial variation, as shown in Fig. 3. Therefore, the basal steady state solution accurately describes the temperature and concentration fields only when the axial gradient of the dendrite area is not largely negative. This region is represented by the solid portion of the curves in Fig. 5–7. The dashed portion represents the extrapolation of the basal region solution. Detailed analysis of transport phenomena in the dendrite tip region is given in the accompanying paper [11].

As discussed above, the heat flux at any axial position has two components: the solidification heat flux and the sensible heat flux. These components are given by

$$H_{sol}(Z^*) = R\rho_s L f_s(Z^*) \tag{32}$$

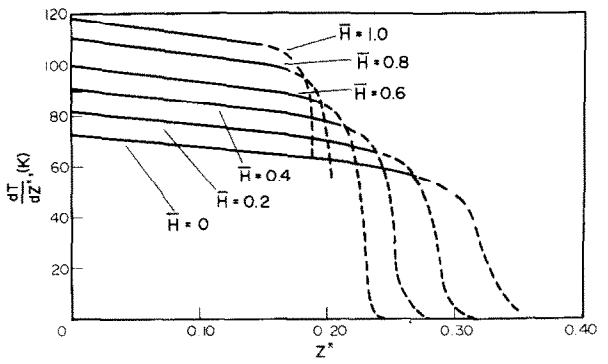

FIG. 7. Temperature gradient profiles vs $\bar{H} = [H(Z^* = 0) - H^*]/H^{max}_{sensible}$.

and

$$H_{\text{sensible}}(Z^*) = R\rho_l \mathscr{C}_l \left\{ [T_\infty - T(Z^*)]\,[1 - f_s(Z^*)] + \int_0^{f_s(Z^*)} T_\infty - T(f_\varphi)\,\mathrm{d}f_\varphi \right\} + R\rho_s \mathscr{C}_s \times \int_0^{f_s(Z^*)} [T(f_\varphi) - T(f_s)]\,\mathrm{d}f_\varphi. \quad (33)$$

where $T(f_s)$ is the temperature at the axial position where the solid fraction is f_s. The first term in equation (33) is the energy flux necessary to change the liquid temperature to the solidification temperature, and the second is the flux required to sub-cool the solid. Both the sensible and the solidification components contribute to the axial variation in the heat flux, but the solidification component is dominant.

The effect of T_∞ and C_∞ on the basal region solution is by way of equations (25) and (33). The value of f_s at $Z^* = 0$ is dictated by the free-field concentration as shown in equation (26). Increasing the free-field concentration decreases the basal dendrite width. However, it will be shown in the accompanying paper that the free-field concentration has little effect on the overall dendrite shape. Increasing T_∞ requires a larger value of $\bar{H}$ to maintain a given dendrite shape as given by equation (33). Note that the overall effect of T_∞ and C_∞ will be considered when the basal solution is "matched" to the dendrite tip solution in the accompanying paper.

The steady state solution predicts that the small variation in the dendrite cross-sectional area is almost linear with axial position in the region near the basal plane (see Fig. 5), and is closely followed by a similar small decrease in the heat flux, in agreement with equation (32). The temperature profiles are nearly linear in this region since the temperature gradient (proportional to the heat flux) changes by only a small amount.

The physical significance of the characteristic length L^* may be explained as follows. The numerator of equation (20) is an equivalent thermal conductivity at the basal plane weighted with respect to the relative amount of solid and liquid present. The denominator is the freezing rate R multiplied by an equivalent specific heat, weighted in a manner similar to the conductivity. With these definitions, equation (20) becomes

$$L^* = \frac{K_{eq}}{R(\rho\mathscr{C})_{eq}} \quad (34)$$

where K_{eq} and $(\rho\mathscr{C})_{eq}$ are the equivalent thermal conductivity and volumetric specific heat as defined above. With these parameters, the non-dimensional axial variable becomes

$$Z^* = \frac{ZR(\rho\mathscr{C})_{eq}}{K_{eq}}. \quad (35)$$

This combination of variables is the Peclet number using Z as the characteristic length.

In equation (34), the quantity $R(\rho\mathscr{C})_{eq}$ is proportional to the convective heat flux and the quantity K_{eq}/L^* is proportional to the conductive heat flux. It can be seen that L^* is the *equivalent axial conduction length* at which the convective and conductive energy fluxes are equal. Using the data of Table 1 and a typical freezing rate of 10^{-3} m/s, the value of L^* is on the order of 10^{-3} m. The reader should note from equation (34) that as the rate of freezing increases, the equivalent conduction length decreases proportionately.

A unique characteristic of the dendrite shape profiles, shown in Fig. 5 is the sudden reduction in dendrite area within a small interval of Z^*. The location of this interval, which depends upon the imposed basal heat flux $\bar{H}$, varies from about $Z^* = 0.18$ to $Z^* = 0.3$. It will be shown in the accompanying paper [11] that the value of Z^* at the actual tip of the dendrite is nearly within the area reduction interval. Further, since Z was non-dimensionalized with respect to $1/R$ [see equation (20)], it follows that dendrite length is proportional to 1/R.

When the basal heat flux is about $H^* + 0.7\,H^{\max}_{\text{sensible}}$,

Table 1. Physical constants for freezing of normal saline

Quantity	Symbol	Value
Density of solid	ρ_s	912 kg/m^3
Density of liquid	ρ_ℓ	998 kg/m^3
Thermal conductivity of solid	k_s	2.21 N-m/s-m-K
Thermal conductivity of liquid	k_ℓ	0.588 N-m/s-m-K
Specific heat of solid	$\mathscr{C}_s$	1.92×10^3 N-m/kg-K
Specific heat of liquid	$\mathscr{C}_\ell$	4.43×10^3 N-m/Kg-K
Diffusion coefficient	D	1.29×10^{-9} m^2/s
Latent heat of fusion	L	0.334 MN-m/kg
Free-field concentration	C_∞	145 g-mol/m^3
Eutectic concentration	C_{eut}	4800 g-mol/m^3
Freezing point equation coefficients	a'	273.2 K
	b'	3.37×10^{-3} K-m^3/g-mol
	c'	2.85×10^{-8} K-m^6/(g-mol)^2
	d'	4.57×10^{-11} K-m^9/(g-mol)^3

the extrapolation of the basal region solution indicates that the heat flux goes to zero just as the solid fraction f_s goes to zero. Under this condition, the energy removal is just sufficient to remove the necessary sensible heat and latent heat of fusion. Reducing the heat flux below this "critical" value provides insufficient energy removal for complete solidification.

SUMMARY AND CONCLUSIONS

Equations describing the axial solute and energy transport during dendritic solidification of aqueous solutions have been derived. Dimensional analysis of these equations yielded a non-dimensional axial coordinate in which the transport fields do not depend upon the rate of growth of the dendrite. Actual dendrite length is inversely proportional to the rate of freezing.

The solution of the solute and energy transport equations depends explicity upon the free-field concentration and on the basal heat flux. As the free-field concentration is increased, the basal dendrite width (diameter) decreases proportionately, but other geometric factors remain unchanged. The basal heat flux necessary to remove the latent and sensible heat is about $H^* + 0.7H^{\max}_{\text{sensible}}$. Increasing the basal heat flux beyond this value decreases the dendrite length and "compresses" the temperature and concentration fields. Reducing the heat flux below $H^* + 0.7H^{\max}_{\text{sensible}}$ provides insufficient energy removal for complete solidification. The influence of the free-field temperature on the overall solution will be demonstrated in the following paper.

Acknowledgements—Support of this work was provided by the Whittaker Health Sciences Fund at the Massachusetts Institute of Technology. The authors also gratefully acknowledge the assistance of Ms. P. Stameris.

REFERENCES

1. B. Chalmers, *Principles of Solidification*, John Wiley, New York (1964).
2. M. C. Flemings, *Solidification Processing*, McGraw-Hill, New York (1974).
3. D. Walton, W. A. Tiller, J. W. Rutter and W. C. Winegard, Instability of a smooth solid–liquid interface during freezing, *Trans. Am. Inst. Min. metall. Engrs* **1,** 1023–1028 (1955).
4. W. A. Tiller and J. W. Rutter, The effect of growth conditions upon the solidification of a binary alloy, *Can. J. Phys.* **34,** 96–107 (1956).
5. W. W. Mullins and R. F. Sekerka, Morphological stability of a particle growing by diffusion or heat flow, *J. appl. Phys.* **31,** 323–329 (1963).
6. W. W. Mullins and R. F. Sekerka, Stability of a planar interface during solidification of a dilute binary alloy, *J. appl. Phys.* **35,** 126–131 (1963).
7. R. F. Sekerka, A stability function for explicit evaluation of the Mullins–Sekerka interface stability criterion, *J. appl. Phys.* **36,** 461–470 (1965).
8. M. G. O'Callaghan, E. G. Cravalho and C. E. Huggins, instability of the planar freeze front during solidification of an aqueous binary solution, *Trans. ASME, J. Heat Transfer*, **102,** 673–677 (1980).
9. G. P. Ivantsov, *Dokl. Akad. Nauk. SSSR* **58,** 567 (1947); translation, "Growth of Crystals," Consultants Bureau, New York (1958).
10. G. F. Bolling and W. A. Tiller, Growth from the melt. III. Dendritic growth, *J. appl. Phys.* **32,** 2587–2605 (1961).
11. M. G. O'Callaghan, E. G. Cravalho and C. E. Huggins, An analysis of the heat and solute transport during solidification of an aqueous binary solution—II. Dendrite tip region, *Int. J. Heat Mass Transfer* **25,** 563–573 (1982).
12. J. P. Terwilliger and S. F. Dizio, Salt rejection phenomena in the freezing of saline solutions, *Chem. Engng. Sci.* **25,** 1331–1349 (1970).

ANALYSE DU TRANSFERT DE CHALEUR ET DE SOLUTE PENDANT LA SOLIDIFICATION D'UNE SOLUTION AQUEUSE BINAIRE—I. REGION PLANE DE BASE

Résumé—On développe une étude mathématique de la solidification permanente, dendritique d'une solution aqueuse binaire. Les équations de transport d'énergie et de soluté sont résolues d'abord dans une zone proche du plan de base, puis indépendamment dans une zone proche des extrémités des dendrites pour obtenir des familles des profils de température, de concentration et de forme de dendrites dans chaque région. On emploie des critères géométriques et thermodynamiques pour déterminer les profils spécifiques dans chaque région qui sont mutuellement compatibles et satisfont les conditions aux limites. Les phénomènes de transfert de chaleur et de masse près du plan de base sont analysés ici, alors que le texte suivant concerne la région des sommets.

Les résultats de l'analyse de la région de base indiquent que la solidification à grande vitesse (grand flux de chaleur à la base) produit des dendrites courtes qui sont plus émoussées. Une variable adimensionnelle de similarité axiale est trouvée qui décrit les champs de température et de concentration indépendant de la vitesse de solidification.

EINE ANALYSE DES WÄRME- UND STOFFTRANSPORTS BEIM ERSTARREN EINER WÄSSRIGEN BINÄREN LÖSUNG—I. BASISFLÄCHEN-BEREICH

Zusammenfassung—Es wird eine mathematische Analyse des stetigen dendritischen Erstarrens einer wäßrigen binären Lösung entwickelt. Die Energie- und Transportgleichungen des gelösten Stoffes werden durch Anwendung einer einfachen Zwei-Zonen-Methode gelöst. Bei diesem Vorgehen werden die gekoppelten Energie- und Stofftransport-Gleichungen zuerst für eine Zone in der Nähe der Basisfläche und dann unabhängig voneinander für eine Zone nahe den Spitzen der Dendriten gelöst. Dabei ergeben sich für jedes Gebiet Familien von Temperatur-, Konzentrations- und Dendritenform-Profilen. Geometrische und thermodynamische Anpassungs-Kriterien, die gegenseitig verträglich sind und die gesamten Randbedingungen erfüllen, werden zur Bestimmung der spezifischen Temperatur-, Konzentrations- und Dendritenform-Profile in jedem Gebiet angewandt. In der vorliegenden Arbeit werden die Wärme- und Stofftransport-Phänomene an der Basisfläche analysiert, während die Untersuchung des Gebiets der Dendritenspitzen und die entsprechende Anpassungs-Prozedur in einem begleitenden Aufsatz ausgeführt werden. Die Analyse des Basisflächengebiets zeigt, daß die Erstarrung bei größeren Boden-Wärmestromdichten kürzere und stumpfere Dendriten hervorruft. Eine dimensionlose axiale Ähnlichkeitsvariable wurde gefunden, die die Temperatur- und Konzentrationsfelder unabhängig von der Gefrier-Geschwindigkeit beschreibt.

АНАЛИЗ ПЕРЕНОСА ТЕПЛА И МАССЫ РАСТВОРЕННОГО ВЕЩЕСТВА ПРИ ЗАТВЕРДЕВАНИИ ВОДНОГО БИНАРНОГО РАСТВОРА — I. ОБЛАСТЬ БАЗИСНОЙ ПЛОСКОСТИ

Аннотация — Проведен математический анализ процесса стационарного дендритного затвердевания водного бинарного раствора. Уравнение переноса энергии и массы растворенного вещества решались простым «двухзонным» методом. При использовании этого метода, для того чтобы получить распределения температур и концентраций, а также формы дендритных ответвлений, уравнения энергии и массы решаются сначала совместно для зоны, расположенной вблизи базисной плоскости, а затем по отдельности для зоны у дендритных вершин. С помощью геометрических и термодинамических критериев сращивания определяются удельные температура и концентрация, а также профили дендритных ответвлений в каждой из ряда схожих зон, в которых выполняются общие граничные условия. В первой части работы анализируются явления тепло- и массопереноса на базисной плоскости, а во второй — процессы в области у вершины дендритов и методика сращивания.

Анализ базисной области показал, что при более интенсивном затвердевании (большая плотность теплового потока) происходит образование менее высоких и более пологих дендритов. Выведена безразмерная осевая автомодельная переменная, с помощью которой можно описывать температурные и концентрационные поля без учета интенсивности затвердевания.